Chemical Engineering Journal 149 (2009) 455–462

Contents lists available at ScienceDirect

Chemical Engineering Journal

journal homepage: www.elsevier.com/locate/cej

Production of carbon nanotubes from methane
Use of Co-Zn-Al catalysts prepared by microwave-assisted synthesis

P. Benito [a], M. Herrero [a], F.M. Labajos [a], V. Rives [a], C. Royo [b], N. Latorre [b], A. Monzon [b,*]

[a] Department of Inorganic Chemistry, University of Salamanca, 37008 Salamanca, Spain
[b] Department of Chemical and Environmental Engineering, Institute of Nanoscience of Aragon (INA), University of Zaragoza, 50009 Zaragoza, Spain

ARTICLE INFO

Article history:
Received 25 September 2008
Received in revised form 16 February 2009
Accepted 17 February 2009

Keywords:
Hydrotalcite
Microwave
Hydrothermal
Catalytic methane decomposition
CCVD
MWNT
Carbon nanotubes
Carbon nanofibers
Co-Zn-Al catalyst

ABSTRACT

Co-Zn-Al mixed oxides obtained from layered double hydroxide (LDH) precursors were synthesized and tested in the formation of multi-walled carbon nanotubes (MWNTs) by catalytic chemical vapour deposition (CCVD) of methane. The precursors were synthesized by co-precipitation from Co, Zn and Al nitrates with carbonate and submitted to microwave-hydrothermal treatment, in order to study the effect of time treatment on the catalyst performance. The microwave ageing treatment does not only play a role on some features of the precursors, such as crystallinity and textural properties, but also on the properties of the catalysts obtained by controlled calcination. The microwave-hydrothermal treatment affects to the distribution of the cations within the layers because of an improved ordering and this effect leads to better dispersed active species in the catalyst. In this sense, it was found that the aged catalysts reach better activity and stability levels during the methane decomposition reaction. Furthermore, the duration of microwave-hydrothermal treatment also produces a change of the kind of carbon nanofilaments produced. When the catalyst is not aged, herringbone carbon nanofibers (diameter ~14 nm) were found. On the other hand, multi-walled carbon nanotubes (diameter ~20–30 nm) could be observed in the sample after reaction with the 300 min aged catalyst. Finally, the application of a kinetic model based on the growing mechanism of nanocarbonaceous materials (NCMs), allows determining the influence of the microwave-hydrothermal treatment time on the kinetic parameters.

1. Introduction

The study of carbon nanotubes (CNTs) has attracted considerable attention in recent years, not only due to the remarkable physical and chemical properties of these materials, but also because of the wide range and versatility of their potential applications [1]. Catalytic chemical vapour deposition (CCVD), arc discharge and laser ablation remain the three major synthesis routes for CNT production. CCVD process is expected to strongly decrease the production costs of CNT since it is easy to scale up and suitable for continuous operation. Besides, it offers a higher rate of carbon growth and ease of controlling reaction conditions. The role of the catalyst is crucial to get high selectivity towards high quality CNT with narrow diameter distribution [2,3].

On the other hand, catalytic methane decomposition (CMD) is an alternative route to steam reforming for the production of hydrogen [4–6]. It is a moderately endothermic reaction (ΔH_{298} = 74.5 kJ/mol CH_4), which produces hydrogen as a unique gaseous product, avoiding direct CO_2 formation and also, the subsequent steps of CO removal [7]. Several techno-economic studies about this process [8,9] conclude that economically as well as from the energetic efficiency, this is a much more interesting route than steam reforming.

Hydrogen is a clean fuel that emits no CO_2 when burned or used in H_2–O_2 fuel cells, can be stored as a liquid or a gas, is distributed via pipelines, and has been described as a long-term replacement for natural gas [10–12]. Therefore, a growing demand is forecast in all sectors, including petroleum refining where the increasing need to process heavy and high-sulphur content crude-oil is accompanied with the lowering of hydrogen co-product in the catalytic reforming process.

The role of the catalyst is crucial to get high activity and, specially, selectivity towards CNT formation. Fe, Co, and Ni, as well as their alloys are the active metals usually utilized in the composition of the catalyst used in this process [13–16]. Layered double hydroxides (LDHs) are a class of synthetic anionic clays whose structure can be described as follows: brucite-like layers, $Mg(OH)_2$, in which some of the divalent cations have been isomorphically replaced by trivalent ones, giving rise to positively charged sheets, electrical neutrality is maintained by the anions located in the interlayer region in which water molecules are also found [17]. In this kind of compounds, metal cations can arrange uniformly in the brucite-like layer at an atomic level. Furthermore, an interesting aspect of

* Corresponding author.
E-mail address: amonzon@unizar.es (A. Monzon).

1385-8947/$ – see front matter © 2009 Elsevier B.V. All rights reserved.
doi:10.1016/j.cej.2009.02.022

Table 1
Chemical formulae, crystallite size (D), specific surface area and pore volume for the LDH precursors.

Sample	Formulae	D (Å)	S_{BET} ($m^2\,g^{-1}$)	V_p ($cm^3\,g^{-1}$)
CZA0	$[Co_{0.26}Zn_{0.25}Al_{0.49}(OH)_2](CO_3)_{0.245}$	119	81	0.2142
CZAW10	$[Co_{0.25}Zn_{0.26}Al_{0.49}(OH)_2](CO_3)_{0.245}$	190	70	0.1631
CZAW30	$[Co_{0.26}Zn_{0.25}Al_{0.49}(OH)_2](CO_3)_{0.245}$	236	58	0.1134
CZAW60	$[Co_{0.26}Zn_{0.26}Al_{0.48}(OH)_2](CO_3)_{0.240}$	275	59	0.1075
CZAW300	$[Co_{0.27}Zn_{0.26}Al_{0.47}(OH)_2](CO_3)_{0.235}$	421	38	0.0638

LDHs chemistry is their use as catalysts after a controlled thermal treatment, generally around 450–550 °C [18–24]. At these temperature LDHs lose their layered structure and form mixed metal oxides with, high surface area, high dispersion of metal cationics and small crystal size. Since stable metal particles can be obtained by the subsequent reduction of the calcined LDHs [25], it is possible to use cobalt-containing LDH materials, as alternative catalyst precursors for the synthesis of multi-walled carbon nanotubes (MWNTs).

In the present contribution we have prepared layered double hydroxides with Co, Zn and Al in the brucite-type sheets as precursors of mixed oxides in order to stabilise Co^{2+} clusters, modulating the amount of Co. The microwave radiation was used as a source of heating to prepare well crystallized materials and in order to avoid cobalt oxidation [26,27]. This method provides particle size homogeneity of the solids obtained and additional advantages: reduction of the time required and a save in energy [28]. These improvements are a consequence of the fast and homogeneous heating of the material upon its exposure to the microwave radiation. Moreover, it has been shown that the microwave-hydrothermal treatment modifies the properties of the products obtained upon thermal decomposition of ZnCoAl LDHS [27]. Thus here, Zn, Co, Al catalysts obtained by thermal decomposition of LDHs submitted to microwave-hydrothermal treatment have been tested in the methane decomposition reaction. The samples before and after reaction have been characterized with the aim of studying the effect of the pre-treatment on the catalytic performances and observing the changes in the catalyst structure and the type of carbon produced. Finally, a kinetics model of mechanistic character [23,29] for explaining the growing mechanism of nanocarbonaceous materials (NCMs) has been used to analyse the influence of the aging time on the values of intrinsic kinetics parameters.

2. Experimental

2.1. Synthesis of the solids

The solids were prepared by co-precipitation, by mixing an aqueous solution containing chlorides of the metal cations (Co, Zn and Al) in the desired amounts, with an aqueous solution of Na_2CO_3 and NaOH at room temperature. The pH of the reaction mixture was kept at pH 9.5 by adding 1 M NaOH with a pH-Burette 240 from Crison. The molar ratios used were $Co^{2+}/Zn^{2+}/Al^{3+} = 1:1:2$. The slurry obtained was submitted to microwave-hydrothermal treatment at 125 °C for 10, 30, 60 and 300 min in a Milestone Ethos Plus multimode cavity microwave oven as reported elsewhere [27]. In all cases, the precipitates were washed and dried at 40 °C in an open air oven.

The materials were calcined at 500 °C under a nitrogen flow following a 5 °C min^{-1} ramp, with three steps: at 180 °C (1 h), 300 °C (1 h) and 500 °C (11 h), resulting in catalytic materials.

2.2. Characterization of the solids

Element chemical analysis for Co, Zn and Al was carried out by atomic absorption in a Mark 2 ELL-240 apparatus, in Servicio General de Análisis Químico Aplicado (University of Salamanca, Spain). Powder X-ray diffraction (PXRD) patterns were recorded in a Siemens D-500 instrument using Cu-Kα radiation (λ = 1.54050 Å) and equipped with Diffract AT software. Identification of the crystalline phases was made by comparison with the JCPDS files [30]. UV–vis spectra were recorded following the diffuse reflectance (DR/vis–UV) technique in a PerkinElmer Lambda 35 instrument with a Labsphere RSA-PE-20 integrating sphere and software UV WinLamb, using 2 nm slits and MgO as reference. Differential thermal analyses (DTA) were carried out in a DTA-7 instrument from PerkinElmer, in flowing oxygen and/or nitrogen (from L' Air Liquide, Spain), at a heating rate of 10 °C min^{-1}. Specific surface assessment was carried out in a Gemini instrument from Micromeritics. The sample (ca. 80–100 mg) was previously degassed in flowing nitrogen at 110 °C for 2 h in a FlowPrep 060 apparatus, also from Micromeritics, in order to remove physisorbed water, and the data were analysed using published software [31]. Temperature-programmed reduction (TPR) analysis was carried out in a Micromeritics 2900 TPD/TPR instrument. The reducing agent was H_2/Ar (5 vol%) from L' Air Liquide (Spain) and the gas flow (50 ml min^{-1}), sample weight (15–20 mg), and heating schedule (10 °C min^{-1}) were chosen according to the literature [32] to optimize resolution of the curves. Calibration of the instrument was carried out with CuO (from Merck).

2.3. Catalytic tests

Methane decomposition reaction was carried out in gas phase by using a thermobalance (CI Electronics Ltd., UK, model MK2) operated as a differential reactor. This experimental system allows continuous recording of the sample weight and temperature during reaction. Catalyst reduction was carried out *in situ* at 700 °C for 2 h using a H_2 (40%)/N_2 mixture. Reaction conditions were as follows – sample weight: 100 mg; temperature: 625 °C; total flow rate: 750 Nml/min; feed composition (%CH_4/%H_2/%N_2): 5/2/93. After reaction, the reactor was cooled down to room temperature in a N_2 atmosphere.

2.4. Catalyst and carbon characterization after reaction

The catalysts as well as the carbon obtained were characterized by transmission electronic microscopy (TEM) and X-ray diffraction (XRD). TEM images were carried out in a JEOL-2000 FXII microscope, in the Electronic Microscopy Service of University of Zaragoza. The powder X-ray diffraction pattern was recorded within the range 5–85° (2θ) by a Rigaku/Max Cu rotatory anode equipment.

3. Results

3.1. Characterization of the catalysts

3.1.1. Characterization of the LDH precursors

The effect of microwave-hydrothermal treatment on the properties of the LDH precursors is similar to that previously observed [33]. In all cases, the M^{2+}/M^{3+} and Co/Zn ratios are reasonably coincident with the ratios in the starting solutions (Table 1). A fast enhancement of the crystallinity is observed during the microwave treatment because of the rapid volumetric heating [28]. It should be

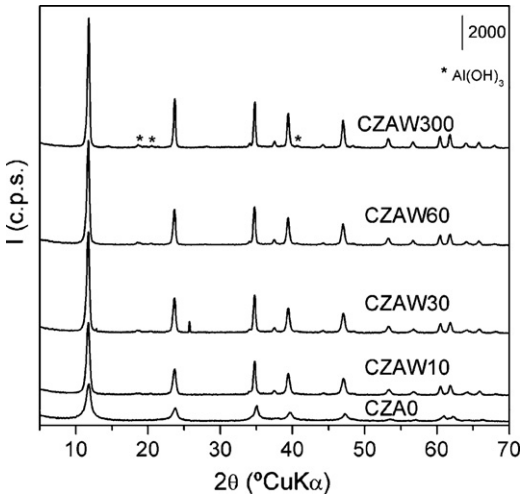

Fig. 1. PXRD patterns of the LDH precursors (all peaks, unless those marked, are due to the hydrotalcite-type phase).

noted the evolution of the PXRD patterns – diffraction lines become sharper and more symmetric – and the crystallite size (Table 1) from the fresh to the 300 min irradiated sample (Fig. 1). Small diffraction peaks are observed at ca. $2\theta = 18.6$ and 20.3 due to $Al(OH)_3$, since the $M^{2+}/M^{3+} = 1/1$ ratio is outside of the range of formation of pure LDHs. Neither segregation of crystalline ZnO nor Co_3O_4 phases was detected; however, the presence of amorphous phases cannot ruled out. In fact, DR/vis–UV spectra, Fig. 2, shows along the microwave-hydrothermal treatment a steady increase of the absorption in the wavelength range from 600 to 800 nm, together with a decrease in the intensity of the maximum close to 550 nm, pointing to a slight oxidation of Co^{2+} to Co^{3+}. This behaviour is opposite to results previous reported [26], and it could be related to the M^{2+}/M^{3+} ratio of the LDHs.

The Ostwald ripening mechanism taking place during microwave ageing also leads to the modification of the textural properties of the solids. The N_2 adsorption/desorption isotherms of all solids belong to the type II of the IUPAC classification for non porous or macroporous lamellar materials [34]. Furthermore, the absorption–desorption isotherms exhibit a type H3 hysteresis loop, attributed to the presence of slit-shaped pores. The narrowing of the hysteresis loops at increasing periods of time, suggested a

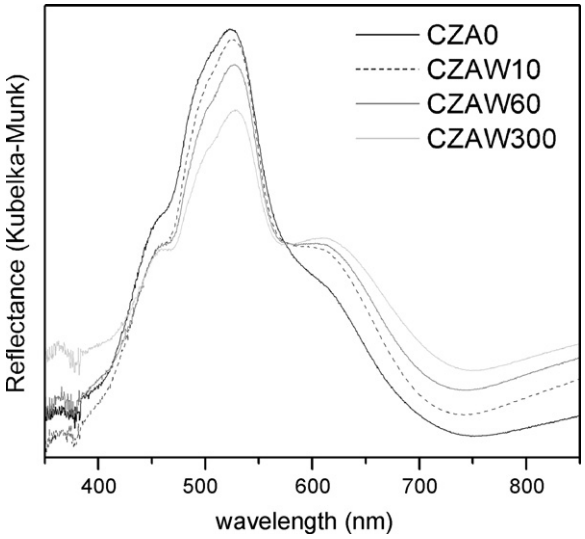

Fig. 2. DR/vis–UV spectra of the synthesized LDHs.

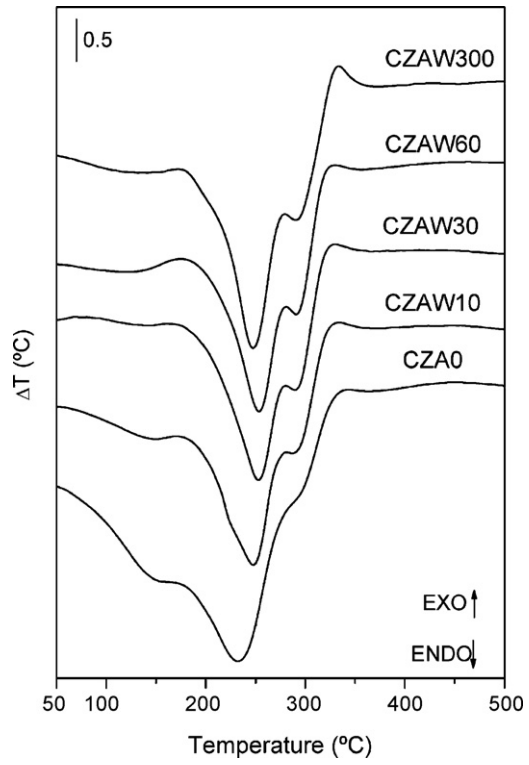

Fig. 3. DTA curves for all the samples.

cancelation of the porous structure because of the steady growing of the LDH particles. The S_{BET} data, displayed in Table 1, also agree with the formation of larger particles which leads to a lower aspect ratio values, that is, lower specific surface values.

Similarly, the thermal stability of the samples depends on the crystallinity degree of the solids [35,36]. DTA curves (Fig. 3) are characteristic of Co, Zn, Al LDHs [27]. The profiles show a single endothermic effect with minimum around 230–250 °C, depending on the specific sample, with two shoulders both at higher and lower temperatures, indicating that the water loss and the lamellar collapse take place almost simultaneously. Finally, a small exothermic effect is recorded at ca. 330 °C, ascribed to an oxidation process [37,38]; since this process occurs simultaneously with thermolysis of the solid and carbonate and hydroxyl removal (endothermal), they cancel each other out to some extent [39]. The fresh sample,

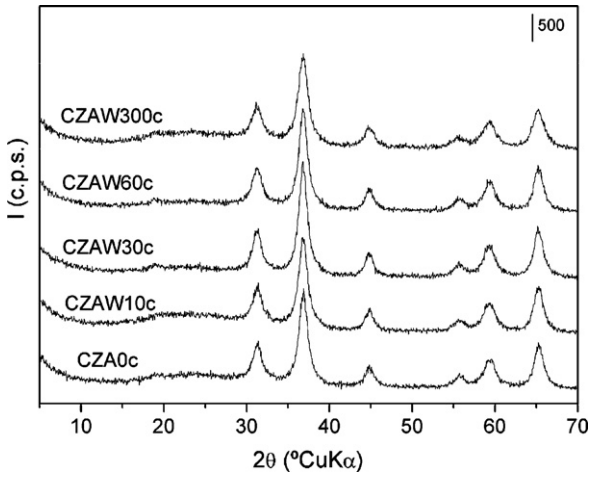

Fig. 4. PXRD patterns of the calcined samples.

Table 2
Lattice parameters (a, Å) and crystallite size (D, Å), both as measured from diffractions (2 2 0) and (3 1 1), and specific surface area and pore volume for the calcined LDHs.

Sample	a(2 2 0)	a(3 1 1)	D(2 2 0)	D(3 1 1)	S_{BET} ($m^2\,g^{-1}$)	V_p ($cm^3\,g^{-1}$)
CZA0c	8.070	8.064	81	79	110	0.3089
CZAW10c	8.084	8.086	78	73	121	0.2572
CZAW30c	8.096	8.108	83	77	111	0.1995
CZAW60c	8.096	8.086	65	76	112	0.1969
CZAW300c	8.123	8.108	69	67	105	0.1426

CZA0, shows the broadest endothermic effect, the low temperature shoulder is rather intense, whereas the one at higher temperatures is less defined; moreover, the exothermic effect is hardly detected. For the aged samples, a continuous decrease in the intensity of the first shoulder is observed; the peak around 330 °C is better resolved and the intensity of the exothermic effect increases, and the peak becomes sharper and shifts towards higher temperatures. Note that the most remarkable differences are found on comparing the fresh with the short time aged samples.

3.1.2. Characterization of the catalysts

PXRD patterns show the diffraction peaks corresponding to a spinel-like phase, Fig. 4. The single oxides CoO or ZnO are not identified by PXRD in the catalysts, although the presence of some amorphous material or highly dispersed oxide particles cannot be discounted entirely. As these solids are poorly crystallized, it is not possible to identify through this technique which spinel phase is precisely formed. However, the tendency of Co and Zn to form a spinel-like structure should be taken into account; as the tendency of cobalt to occupy the octahedral sites is very high, the most feasible structures to be obtained after the calcination treatment could be Co_3O_4, $ZnCo_2O_4$ and $Co(Co,Al)_2O_4$ [40]. On comparing the patterns of all the calcined solids and the crystallite sizes calculated by the Scherrer equation (Table 2), it seems that the better crystallized LDH precursor, the lesser crystalline degree of the calcination products; however, these differences are not very remarkable.

DR/vis–UV spectra show a high absorption between 400 and 700 nm, and a shoulder which varies depending on the sample is observed up to 1100 nm, Fig. 5. The spectra are very similar to that of the Co_3O_4 spinel phase [26], as the characteristic broad absorption in the 600–750 nm range, due to the transition $^1A_{1g}(I) \rightarrow {}^1T_{1g}(I)$ for a Co^{3+} species in an octahedral environment, is observed in all the spectra. The presence of absorption bands due to divalent cobalt in the spectra cannot be excluded, but the high intensity of the absorption of the trivalent species mask these bands.

Contrary to the behaviour observed for the LDH precursors, very similar S_{BET} (Table 2) values are obtained for all the solids when calcining the LDHs, ranging from 105 to 120 $m^2\,g^{-1}$, regardless of the surface values measured for their precursors. However, the pore volume (V_p) values depend on the post-treatment of the LDHs. A steady decrease in V_p is observed from sample CZA0c to CZAW300c. The shape of the N_2 isotherms is quite different depending on the specific solids, Fig. 6, in agreement with the results previously obtained for mixed oxides with very similar chemical composition and submitted to the same ageing treatment. The CZA0c sample shows a similar isotherm to that of its LDH precursor. For the sample CZAW10c, no differences were observed at low relative pressures; however, the slope raise at high relative pressures indicates an increased uptake of adsorbate due to adsorption in mesopores, which leads to multilayer formation until a given pressure where condensation takes place, accounting for a sharp increase of the adsorbed volume; the pressure at which this process occurs is dependent on the pore size, i.e., for large mesopores it is observed at high pressures. The uptake is shifted towards lower relative pressures for the catalysts derived from the longer microwave treated precursors (Fig. 6). In addition, the shape of the hysteresis loops is different before and after the *plateau*, suggesting the existence of two kinds of pores. A very narrow H3 hysteresis is observed at high pressures, while at lower pressures the adsorption and desorption branches are not parallel, a characteristic behaviour of solids whose pore structures are complex and tend to be made up of interconnected networks of pores of different size and shape, in which both

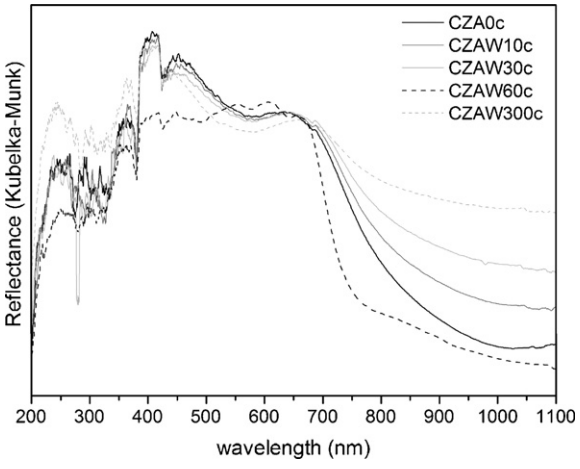

Fig. 5. DR/vis–UV spectra of the calcined solids.

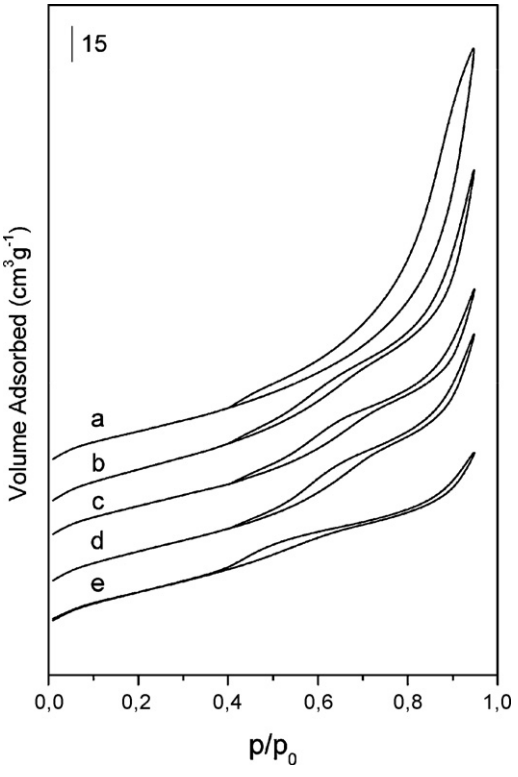

Fig. 6. N_2 adsorption/desorption isotherms of the calcined solids. CZA0c (a), CZAW10c (b), CZAW30c (c), CZAW60c (d), CZAW300c (e).

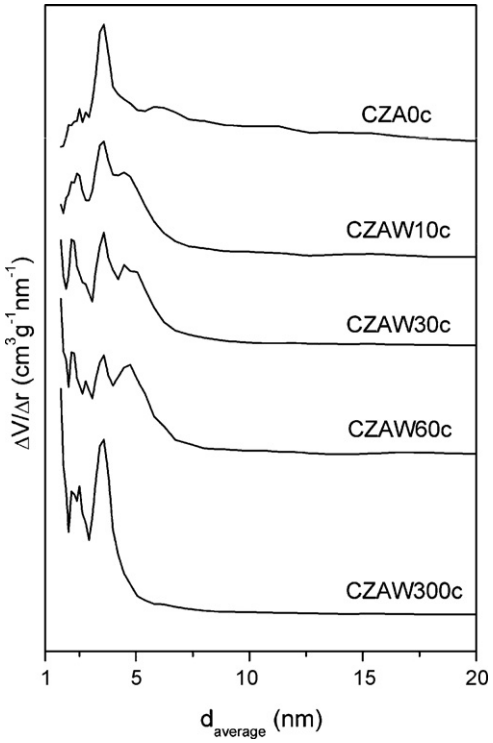

Fig. 7. BJH pore size distribution of all the catalysts.

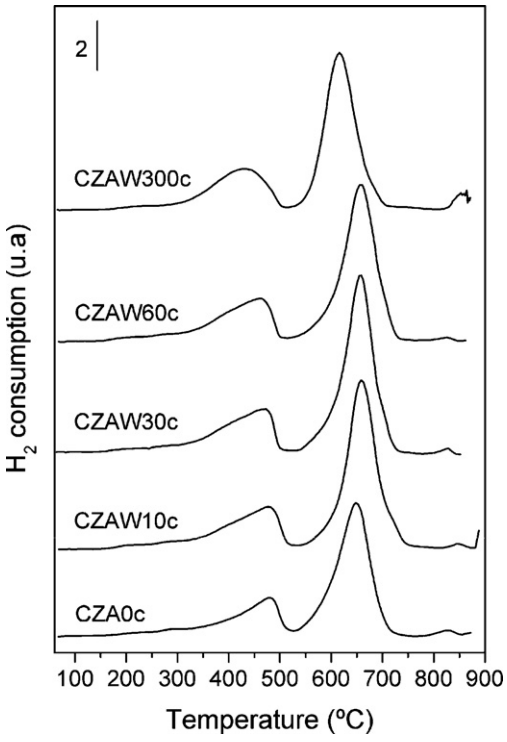

Fig. 8. TPR profiles of the solids calcined at 500 °C.

pore size distribution and pore shape are not well defined [41]. In order to obtain some clues about the pore size distribution of the catalysts, the desorption branch is used in the Barret Joiner Halenda (BJH) method, Fig. 7. The curves reveal significant modifications in the pore size depending on the ageing treatment the LDH precursors were submitted to, as it was suggested from the analysis of the isotherms. Sample CZA0c shows a monomodal distribution with pores around 4 nm. However, in the catalysts derived from the LDHs aged for 10, 30 and 60 min smaller and larger pores are developed with radii around 2.5 and 5 nm. Finally, sample CZAW300c exhibits a bimodal distribution with pores around 2.5 and 3.5 nm, with larger contribution to the adsorption from the latter ones. In order to check the existence of micropores, the *t*-plot method was used, but no micropores were detected.

TPR profiles of the catalysts are shown in Fig. 8. Two reduction maxima are detected for all samples around 450 and 650 °C, pointing to the presence of two cobalt species [41].

The first peak can be ascribed to the reduction of Co_3O_4 which usually occurs in two consecutive steps, $Co_3O_4 \rightarrow CoO \rightarrow Co^0$ [42]; these steps are almost indistinguishable and would explain the broadening of the first TPR peak. Finally, the peak around 650 °C can be associated to the reduction of Co^{2+} strongly interacting with $ZnAl_2O_4$ or forming $CoAl_2O_4$ [43].

3.2. Catalytic activity and carbon nanofilament growth

The activity results obtained for the different catalysts are shown in Fig. 9. Carbon formation rate curves have been calculated from the numerical derivative of the experimental carbon content versus time curves.

It can be observed that all the catalysts are active in the methane decomposition reaction but deactivation is observed on prolonging the reaction. Owing to deactivation, the carbon formation rate curves show an initial period of rapid growth until a maximum is reached. This period is followed by a decrease in the carbon formation rate. During this period of activity decay, the deactivation rate is higher than the filament formation rate [42,44].

Furthermore, it is important to emphasize that the microwave-hydrothermal treatment improves the activity and the stability of the CoZnAl catalyst. In order to quantify the influence of the operating conditions over the amount and the formation rate of the NCMs, we have previously developed a kinetic model for carbon growth

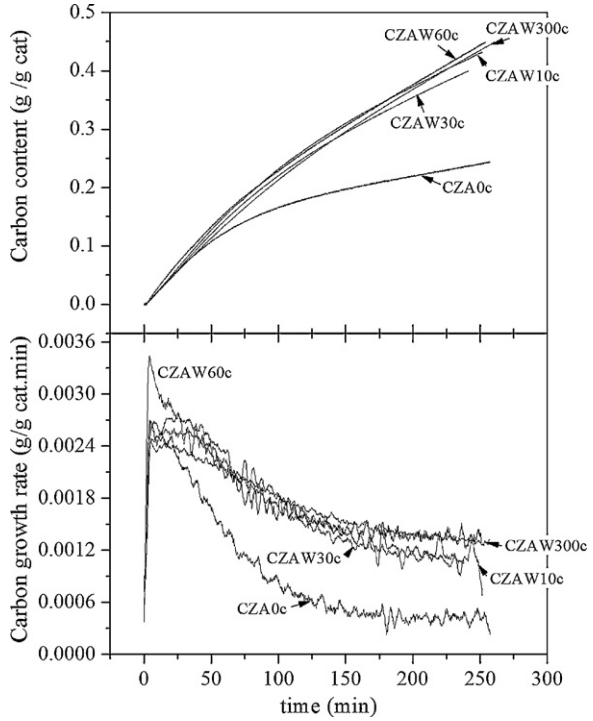

Fig. 9. Evolution with time of the carbon content and carbon growth rate for the CoZnAl catalysts. Reaction temperature: 625 °C; feed composition: 5%CH_4/2%H_2/93%N_2.

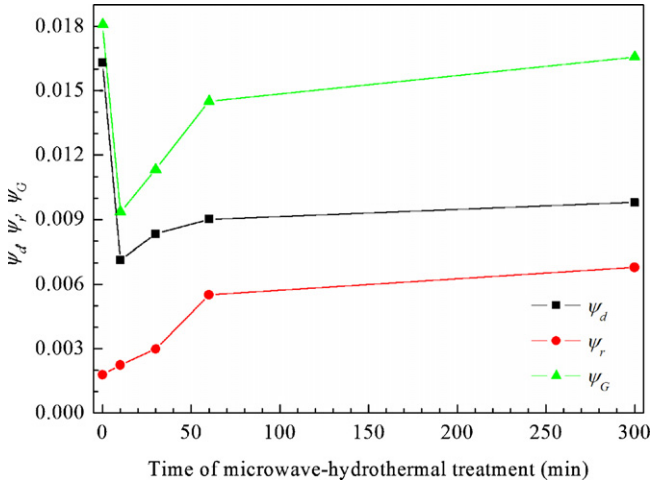

Fig. 10. Influence of microwave-hydrothermal treatment time on the kinetic parameters ψ_d, ψ_r and ψ_G.

during catalytic hydrocarbon decomposition [29,45]. The mathematical description of this kinetic model takes into account the main steps of carbon formation and accumulation over the catalyst: diffusion, nucleation, filament growth and catalyst deactivation. According to this model, the concentration of carbon accumulated over the catalyst, m_C (g C/g cat.), and the carbon formation rate, r_C (g C/(g cat. min)), can be written as follows [29]:

$$m_C(t) = r_{C_0}[a_S t + \alpha_1(1 - \exp(-\psi_G t)) - \alpha_2(1 - \exp(-r_D t))] \quad (1)$$

$$r_C(t) = r_{C_0}[a_S + \psi_G \alpha_1 \exp(-\psi_G t) - r_D \alpha_2 \exp(-r_D t)] \quad (2)$$

where α_1 and α_2 are given by:

$$\alpha_1 = \frac{r_D(1 - a_S)}{\psi_G(r_D - \psi_G)}; \quad \alpha_2 = \frac{(r_D - \psi_G a_S)}{r_D(r_D - \psi_G)}; \quad (3)$$

The kinetic parameters of the model are – r_{C_0}: flux of carbon formation reached at the steady state, in the absence of catalyst deactivation, g carbon/(g cat. min), The term r_{C_0} is the product of the concentration of metallic actives sites times the carbon diffusion coefficient [29]. r_D: intrinsic kinetic rate of methane decomposition over the metallic surface, min^{-1}, ψ_d: deactivation kinetic function, min^{-1} and ψ_r regeneration kinetic function, min^{-1}. These four parameters include the dependence on the reaction temperature (apparent activation energies and pre-exponential factors), the

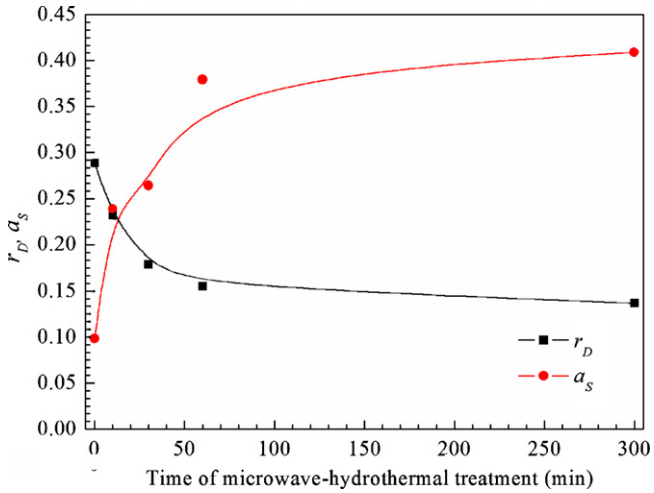

Fig. 11. Influence of the microwave-hydrothermal treatment time on the kinetic parameters r_D and a_S.

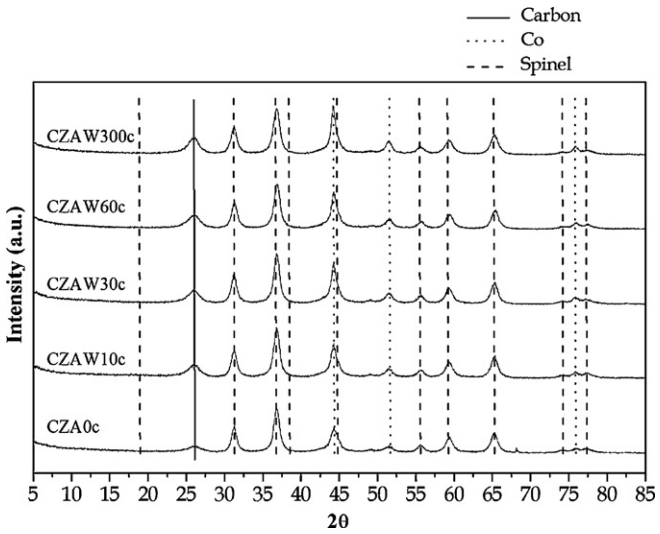

Fig. 12. XRD patterns of the samples after reaction.

atmosphere composition (kinetic orders), and the type and composition of the catalyst (metallic exposed area and intrinsic reactivity).

The term a_S represents the residual activity of the catalyst and, according to the kinetic model, it can be calculated as:

$$a_S = (\psi_r/\psi_G); \quad \psi_G = \psi_d + \psi_r \quad (4)$$

Eq. (1) is directly used to fit the experimental data (Fig. 9) in order to obtain the influence of the microwave-hydrothermal treatment time on the kinetic parameters. There results are presented in Figs. 10 and 11. When the catalyst is not aged under microwave-hydrothermal treatment, r_D, parameter related to the intrinsic methane decomposition rate, is greater (Fig. 11).

However, ψ_d (i.e., deactivation function) is also very high and the regeneration effect (ψ_r) is low (Fig. 10). As a consequence, the catalyst loses its activity after ca. 150 min and the residual activity is very close to zero.

On the other hand, the greater is the time of the microwave-hydrothermal treatment, the higher are the deactivation and regeneration effects. As a result, although r_D decreases, the carbon content obtained is very similar but the residual activity is higher for the solids irradiated longer times.

The mechanism of formation of CNF that has generally been accepted includes methane adsorption on the surface of the reduced metal, gradual dehydrogenation of methane, with the abstraction of the first hydrogen atom from molecularly adsorbed methane as the rate-determining step, conversion of the adsorbed methane to adsorbed surface carbon via surface reactions, subsequent segregation of surface carbon into the layers near the surface, diffusion of carbon through metal particles, and then precipitation on the rear side of the metal particle [45–48]. De Chen et al. [22] proved that, during methane decomposition reaction, MWNT formation rate and encapsulating carbon formation rate (i.e., deactivation rate) deeply depend of metallic size developed after the reduction stage, detecting the existence of an optimal Ni particle size which optimizes the reaction yield. Small Ni particles show low rate of MWNT growth and also rapid encapsulation, as a result of the low driving force produced for carbon diffusion through the Ni crystals [22]. Large Ni crystals have low activity due to the low metallic dispersion. Consequently, surface coverage of carbon increases, enhancing the formation of encapsulating coque and, therefore, the deactivation. This consideration, could explain the observed variation of the rate of MWNT formation, and accordingly of the kinetic parameters, with the samples treated at different microwave-hydrothermal treatments, see Figs. 10 and 11.

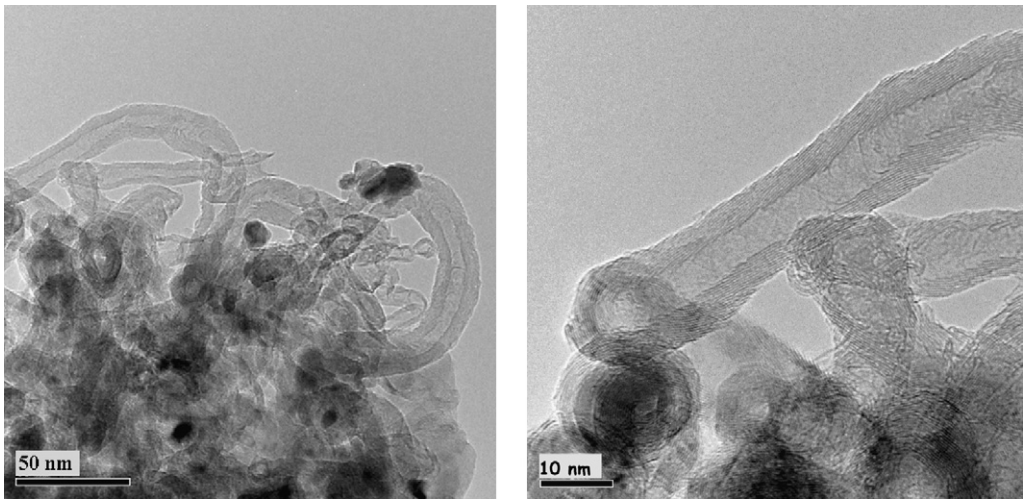

Fig. 13. TEM images of the samples after reaction at 625 °C with 5%CH_4/2%H_2/93%N_2. Catalyst: CZA0c.

As the microwave-hydrothermal treatment increases, initially is observed a strong diminution of ψ_d, a lower decrease of r_D. and an increase of the ψ_r. These variations are consequence of the net increase of the reaction rate showed in Fig. 10. Definitely, the effect of the particle size is consequence of the delicate equilibrium that occurs at the metallic surface between the carbon diffusion through the particles that form the MWNT and that in the model is represented by r_{C_0} and r_D, and the encapsulating effect of the carbon that remains at the surface causing the deactivation, which determine the value of ψ_d.

The rate of carbon precipitation at the rear side of the particles, and therefore, of MWNT growth is determined by the degree of interaction metal-support. If this interaction is modified there is a change in the rate of all the stages of diffusion-precipitation favouring the MWNT growth, if the diffusion is enhanced, or by the contrary favouring the deactivation, if the accumulation of encapsulating coke is promoted. In this last case, if the amount of encapsulating coke increases could increase the rate of gasification with the hydrogen present in the reaction atmosphere, which is considered by the model as an increase of the parameter ψ_r.

3.3. Catalyst and carbon characterization after reaction

The XRD patterns of the reaction products (Fig. 12) show metallic Co^0, formed during the reduction process, and a spinel structure, which indicates that the initial structure of the catalysts does not undergo any substantial degradation during the reaction. In addition, carbonaceous materials (amorphous carbon and polyaromatic carbon typical of graphene-based materials such as carbon nanofibers and multiwall nanotubes) can be observed. The quantities of each type of carbonaceous materials depend on the duration of microwave-hydrothermal treatment [42,49]. The filamentous morphology of the carbon products is demonstrated by the TEM images in Figs. 13 and 14. When the catalyst is not aged under microwave-hydrothermal treatment, the carbon nanofilaments produced correspond to herringbone carbon nanofibers (diameter ~14 nm). In this type of nanofibers, the graphene layers are oriented oblique to the filament axis [50]. On the other hand, multi-walled carbon nanotubes (diameter ~20–30 nm) can be observed in the sample after reaction with the 300 min aged catalyst. In this case, a lower formation of amorphous carbon is observed, in accordance with the higher activity of the catalysts,

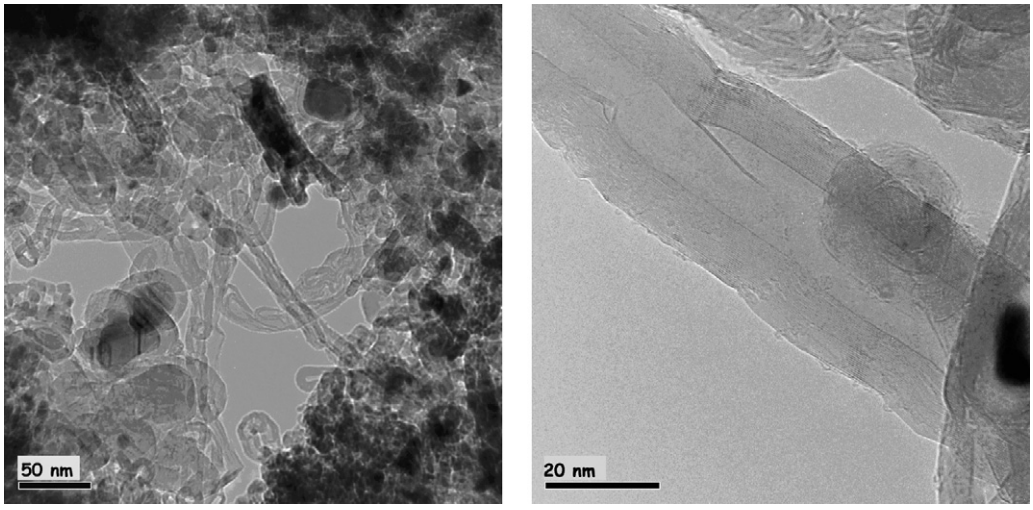

Fig. 14. TEM images of the samples after reaction at 625 °C with 5%CH_4/2%H_2/93%N_2. Catalyst: CZAW300c.

Fig. 9. This fact, as was pointed out above, is due to both a diminution of the intrinsic kinetic deactivation constant and an increase of the kinetic regeneration constant. The results obtained in this work indicate that the microwave-hydrothermal treatment induce some change in the metal-support interaction affecting the catalyst activity, stability and selectivity to different NCMs obtained.

4. Conclusions

A series of CoZnAl catalysts has been studied in this work. The microwave-hydrothermal treatment determines the chemico-physical properties of CoZnAl catalysts obtained by calcination of LDHs at 500 °C. The treatment affects to the distribution of the cations within the layers of the precursors because of an improved order. This effect is also observed in the catalysts. The kinetic study of carbon growth from the catalytic decomposition of methane indicates that the treatment improves the activity and the stability of the CoZnAl catalyst. However, remarkable differences between the different aged catalysts are not found. This observation is in agreement with the results obtained by characterization, the greater changes in the properties are observed for the sample aged for the shortest period of time. On the other hand, the transmission electron microscopy results show that the carbon products obtained also depend on the duration of microwave-hydrothermal treatment, producing a change of the type of nanofilaments formed (herringbone carbon nanofibers or multi-walled carbon nanotubes) and of the quantity of amorphous carbon produced.

The kinetic model developed for carbon filaments formation is based in the reaction mechanism [29]. It fits satisfactorily the experimental data and allows uncoupling an investigating the influence of the microwave-hydrothermal treatment time on each physical stage involved on the process of carbon filaments growth.

Acknowledgements

The authors acknowledge financial support from ERDF, MEC, Madrid, Spain (Projects CTQ 2004-03973/PPQ, CTQ 2007-62545/PPQ and MAT2006-10800-C02-01). P.B. thanks a grant from JCyL.

References

[1] M.S. Dresselhaus, G. Dresselhaus, Ph. Avouris (Eds.), Carbon Nanotubes: Synthesis, Structure, Properties and Applications, Springer-Verlag, Berlin, 2001.
[2] Y. Li, J. Chen, Y. Qin, L. Chang, Energy Fuels 14 (2000) 1188.
[3] G.G. Kuvshinov, D.G. Kuvshinov, A.M. Glushenkov, Chem. Sustain. Dev. 1 (2003) 135.
[4] N.Z. Muradov, Catal. Commun. 2 (2001) 89.
[5] K. Otsuka, S. Takenaka, H. Ohtsuki, Appl. Catal. A: Gen. 273 (2004) 113.
[6] I. Suelves, M.J. Lázaro, R. Moliner, J.L. Pinilla, H. Cubero, Int. J. Hydrogen Energy 32 (2007) 3320.
[7] S.Y. Chin, Y.H. Chin, M.D. Amiridis, Appl. Catal. A: Gen. 300 (2006) 8.
[8] F. Salman, C. Park, R.T.K. Baker, Catal. Today 53 (1999) 385.
[9] C. Pham-Huu, N. Keller, G. Ehret, L.J. Charbonniere, R. Ziessel, M.J. Ledoux, J. Mol. Catal. A 170 (2001) 155.
[10] J.N. Armor, Appl. Catal. A 176 (1999) 159.
[11] R.M. Navarro, M.A. Peña, J.L.G. Fierro, Chem. Rev. 107 (2007) 3952.
[12] R. Moliner, I. Suelves, M.J. Lázaro, O. Moreno, Int. J. Hydrogen Energy 30 (2005) 293.
[13] T. Zhang, M.D. Amiridis, Appl. Catal. A 167 (1998) 161.
[14] G.G. Kuvshinov, Yu.I. Mogilnykh, D.G. Kuvshinov, V.I. Zaikovskii, L.B. Avdeeva, Carbon 36 (1998) 87.
[15] S.B. Sinnott, R. Andrews, D. Qian, A.M. Rao, Z. Mao, E.C. Dickey, F. Derbyshire, Chem. Phys. Lett. 315 (1999) 25.
[16] R. Aiello, J.E. Fiscus, H.C. Loye, M.D. Amiridis, Appl. Catal. A 192 (2000) 227.
[17] V. Rives, Layered Double Hydroxides: Present and Future, Nova Science Publishers, New York, 2001.
[18] A. Vaccari, Catal. Today 41 (1998) 53.
[19] D. Tichit, B. Coq, Cattech 7 (2003) 206.
[20] J.C. Rodriguez, A.J. Marchi, A. Borgna, A. Monzón, J. Catal. 171 (1997) 268.
[21] A. Monzón, E. Romeo, C. Royo, R. Trujillano, F.M. Labajos, V. Rives, Appl. Catal. 185 (1999) 53.
[22] K.O. De Chen, E. Christensen, Z. Ochoa-Fernández, B. Yu, N. Tøtdal, A. Latorre, A. Monzón, Holmen, J. Catal. 229 (2005) 82.
[23] L. Dussault, J.C. Dupin, C. Guimon, M. Monthioux, N. Latorre, T. Ubieto, E. Romeo, C. Royo, A. Monzón, J. Catal. 251 (2007) 223.
[24] D. Tichit, C. Gerardin, R. Durand, B. Coq, Top. Catal. 39 (2006) 89.
[25] O. Lebedeva, D. Tichit, B. Coq, Appl. Catal. A 183 (1999) 61.
[26] M. Herrero, P. Benito, F.M. Labajos, V. Rives, J. Solid State Chem. 180 (2007) 873.
[27] M. Herrero, P. Benito, F.M. Labajos, V. Rives, Catal. Today 128 (2007) 9129.
[28] E.T. Thostenson, T.-W. Chou, Composites: A 30 (1999) 1055.
[29] M. Pérez-Cabero, E. Romeo, C. Royo, A. Monzón, A. Guerrero-Ruíz, I. Rodríguez-Ramos, J. Catal. 224 (2004) 197.
[30] JCPDS: Joint Committee on Powder Diffraction Standards, 1977, International Centre for Diffraction Data, Pennsylvania, U.S.A.
[31] V. Rives, Adsorpt. Sci. Technol. 8 (1991) 95.
[32] P. Malet, J. Caballero, J. Chem. Soc. Faraday Trans. 84 (1998) 2369.
[33] P. Benito, F.M. Labajos, V. Rives, in: R.W. Buckley (Ed.), Progress in Solid State Chemistry Research, Nova Science Publisher Inc., New York, 2007, pp. 173–225.
[34] K.S.J. Sing, D.H. Everett, R.A.W. Haul, L. Moscou, R. Pierotti, J. Rouquerol, T. Sieminiewska, Pure Appl. Chem. 57 (1985) 603.
[35] S. Kannan, A. Narayanan, C.S. Swamy, J. Mat. Sci. 31 (1996) 2353.
[36] S. Möhmel, I. Kurzawski, D. Uecker, D. Müller, W. Gebner, Cryst. Res. Technol. 37 (2002) 359.
[37] M.A. Ulibarri, J.M. Fernández, F.M. Labajos, V. Rives, Chem. Mater. 3 (1991) 626.
[38] Z.P. Xu, H.C. Zeng, Chem. Mater. 12 (2000) 3459.
[39] E. Uzunova, D. Klissurski, I. Mitov, P. Stefanov, Chem. Mater. 5 (1993) 576.
[40] T. Baird, K.C. Campbell, P.J. Holliman, P.J. Hoyle, D. Stirling, B.P. Williams, M. Morris, J. Mater. Chem. 7 (1997) 319.
[41] S. Lowell, J.E. Shields, Powder Surface Area and Porosity, Chapman and Hall, London, 1984.
[42] J.I. Villacampa, C. Royo, E. Romeo, A. Montoya, P. del Angel, A. Monzón, Appl. Catal. A 252 (2003) 363.
[43] A.E. Galetti, M.F. Gomez, L.A. Arrua, A.J. Marchi, M.C. Abello, Catal. Comm. 9 (2008) 1201–1208.
[44] M. Monthioux, L. Noé, L. Dussault, J.C. Dupin, N. Latorre, T. Ubieto, E. Romeo, C. Royo, A. Monzón, C. Guimon, J. Mater. Chem. 17 (2007) 4611.
[45] I. Alstrup, J. Catal. 109 (1988) 241.
[46] R.T.K. Baker, P.S. Harris, R.B. Thomas, R.J. Waite, J. Catal. 30 (1973) 86.
[47] J.-W. Snoeck, G.F. Froment, M. Fowles, J. Catal. 169 (1997) 250.
[48] H. Ogihara, S. Takenaka, I. Yamanaka, E. Tanabe, A. Genseki, K. Otsuka, J. Catal. 238 (2006) 353.
[49] M.L. Toebes, J.H. Bitter, A.J. van Pillen, K.P. de Jong, Catal. Today 76 (2002) 33.
[50] H. Wang, R.T.K. Baker, J. Phys. Chem. B 108 (2004) 20273.